J. Fluid Mech. (1988), *vol.* 190, *pp.* 491–512
Printed in Great Britain

On vortex formation from a cylinder. Part 1. The initial instability

By M. F. UNAL AND D. ROCKWELL
Department of Mechanical Engineering and Mechanics, Lehigh University, Bethlehem, PA 18015, USA

(Received 24 October 1985 and in revised form 6 November 1987)

Vortex shedding from a circular cylinder is examined over a tenfold range of Reynolds number, $440 \leqslant Re \leqslant 5040$. The shear layer separating from the cylinder shows, to varying degrees, an exponential variation of fluctuating kinetic energy with distance downstream of the cylinder. The characteristics of this unsteady shear layer are interpreted within the context of an absolute instability of the near wake. At the trailing-end of the cylinder, the fluctuation amplitude of the instability correlates well with previously measured values of mean base pressure. Moreover, this amplitude follows the visualized vortex formation length as Reynolds number varies. There is a drastic decrease in this near-wake fluctuation amplitude in the lower range of Reynolds number and a rapid increase at higher Reynolds number. These trends are addressed relative to the present, as well as previous, observations.

1. Introduction

Over a century ago, Strouhal (1878) observed vortex shedding from a cylinder, and demonstrated that its dimensionless frequency fD/U remained constant over a range of Reynolds number. Subsequently, von Kármán (1911) drew attention to the remarkably ordered vortex street that persists downstream of the cylinder and proposed a stability criterion for its existence. More recently, investigators have focussed on several features of bluff-body vortex shedding, providing valuable insight into aspects such as longitudinal and lateral spacing of vortices, vortex street drag, universal Strouhal numbers, and related phenomena. The investigations and reviews of Roshko (1954), Abernathy & Kronauer (1962), Morkovin (1964), Bearman (1967), Berger & Wille (1972), Griffin & Ramberg (1974), Gerrard (1978), Sarpkaya (1979), Saffman & Schatzman (1982) and Zdravkovich (1986) provide the reader with a rich panorama of insight.

Regarding the process of large-scale vortex formation behind a bluff body in the subcritical Reynolds number regime, Gerrard (1966) and Wille (1974) describe the traditional viewpoint, which emphasizes the crucial role of negative base pressure. As shown in the simplified schematic of figure 1, the existence of the negative base pressure region (designated by the pressure coefficient C_{p_b}) and the inward spiralling of the vorticity layer originally shed from the surface of the bluff body are mutually compatible. Formation of this vortex involves entrainment of the adjacent irrotational flow. At low and moderate values of Reynolds number, the process of vortex formation exhibits a number of additional complexities, delineated in the foregoing references, most recently by Gerrard (1978). We consider them in the context of the present investigation.

Interpretations of vortex street characteristics which embody the base pressure

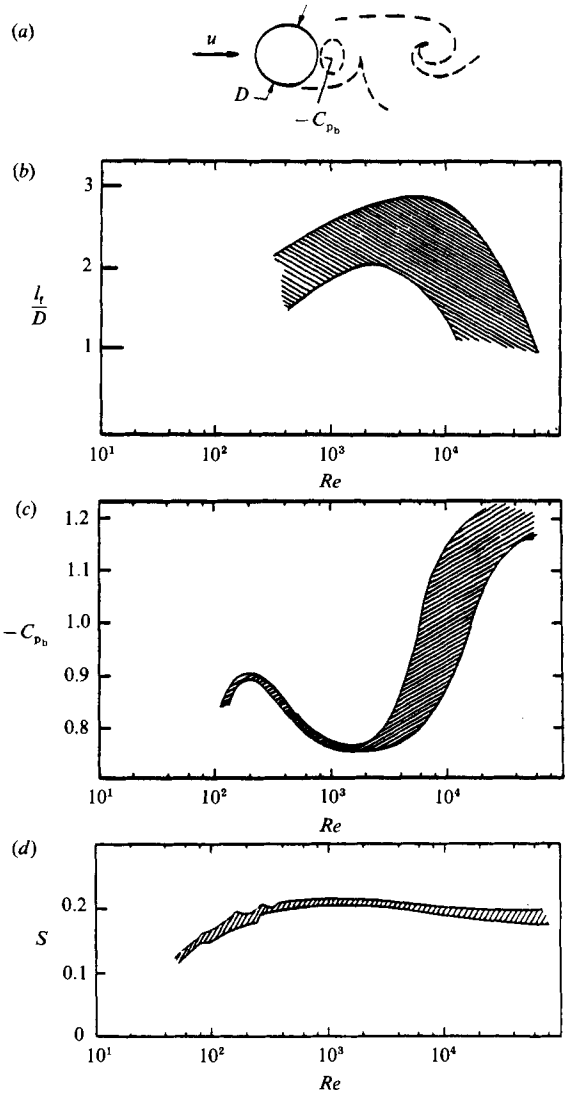

FIGURE 1. Characteristics of vortex shedding from a circular cylinder showing: (*a*) schematic of near-wake region; (*b*) variation of vortex formation length l_f/D as a function of Reynolds number Re; (*c*) variation of base pressure coefficient C_{p_b} with Reynolds number; and (*d*) Strouhal number S as a function of Reynolds number. Cross-hatched regions represent approximate trends based on data in Bloor & Gerrard (1966), Roshko & Fiszdon (1969), Gerrard (1978), and Blevins (1977).

coefficient C_{p_b} have been successful and useful for a number of years (Roshko 1954; Bearman 1967), typically for higher values of Reynolds number than those of interest herein. In general, however, we expect the magnitude of the negative base pressure C_{p_b} to be related to the strength of the vortices formed from the body and the length required to complete their formation, i.e. formation length l_f. Figure 1 (*b*, *c*) shows approximate data bands representing trends of l_f and C_{p_b} with Reynolds number. The reader is referred to Roshko & Fiszdon (1969), Bloor & Gerrard (1966), Gerrard (1978), Blevins (1977) and Zdravkovich (1986), as well as to flow visualization herein, for actual data and their interpretation and limitations. For all

parameters shown in figure 1, there is a degree of uncertainty associated with the character of the free-stream turbulence, cylinder aspect ratio and end effects, and related three-dimensionality. Nevertheless, the trends of the time-averaged data of figure 1 suggest an interrelationship between the magnitude of the base pressure and the vortex formation length.

Figures 1(*b*) and 1(*c*) imply that as the absolute value of the base pressure coefficient decreases, there is an increase in formation length. In figure 1(*c*), the sudden drop in absolute value of base pressure coefficient commencing at $Re \approx 150$–200 may well be associated with the change in character of the vortex shedding to a 'high Reynolds number mode' between Re of about 250 and 500 as described by Gerrard (1966, 1978). According to Gerrard (1978), above Re of about 350, this mode is interrupted by onset of 'transition waves' in the separating shear layer. Moreover, at Re greater than about 300, the vortices from the cylinder rapidly become turbulent; correspondingly, there is an increase in vortex formation length. On the other hand, as the Reynolds number is increased above $Re \approx 1800$, the absolute value of the base pressure increases (figure 1*c*) and the transition waves in the shear layer downstream of the cylinder become particularly evident (Roshko & Fiszdon 1969; Bloor 1964; Gerrard 1978; Wei & Smith 1986).

With regard to examining the vortex development within the framework of linear stability theory, Nishioka & Sato (1978) have studied the disturbance development of the near wake over the Reynolds number range $70 \leqslant Re \leqslant 150$. At sufficiently low Re, $Re = 70$, where the initial fluctuation level near separation is small, they interpret the disturbance growth as classical 'linear growth', corresponding to exponential growth of substantial extent in amplitude of the disturbance. At higher values of $Re = 120$, 150, the initial fluctuation level is relatively large and the streamwise extent of the exponential growth region correspondingly smaller. In fact, they suggest that at sufficiently high values of Re, the exponential growth region would cease to exist altogether. On the theoretical side, they showed that the linear theory of Nakaya (1976) effectively predicted the measured frequency of vortex formation up to $Re = 120$, despite the large fluctuation amplitudes near this upper limit of Re.

In a general sense, truly 'linear' growth of a convective instability in a shear layer occurs up to $\tilde{u}/U$ of, at most, a few per cent, as noted by Ziada & Rockwell (1982), where $\tilde{u}$ is the characteristic (r.m.s.) fluctuation amplitude and U the mean free-stream velocity. Therein, they show that at high amplitudes, higher harmonics are typically present; the growth rates of the fundamental and its higher harmonics are well-predicted by nonlinear theory. Even simple linear theory, however, provides a good approximation for the growth of the fundamental (predominant) disturbance amplitude up to relatively high values of $\tilde{u}/U$. Regarding the initial fluctuation level of the disturbance, there are a variety of forced shear layer experiments (e.g. Freymuth 1966) demonstrating that the rate of exponential disturbance growth of the fundamental does not change significantly with the (forced) amplitude of the disturbance at separation. Therefore, even in cases where the initial level is high due to some sort of forcing, use of linear theory to describe the (albeit short) region of exponential growth of the convective instability may provide a reasonable approximation. In unstable shear flows, one expects the upstream influence from the downstream vorticity dynamics to 'force' the separation region of the cylinder; consequently, the initial fluctuation level in the near-separation region should depend, to some degree, upon the coherence and strength of the downstream vortices. If this upstream influence is sufficiently strong, we expect compatibility

between the eventually formed vortex pattern and the initial region of disturbance amplification.

A particularly important feature of near-wake flows is the possible existence of an absolute, as opposed to a convective, instability (Huerre & Monkewitz 1985). When there exists a region of absolute instability in the flow, one must consider both downstream and upstream waves; in concept, existence of this instability can provide a powerful source of upstream influence, which can lead to a self-sustained feedback loop. In a related study of a geophysical flow, Pierrehumbert (1984) asserts that the flow is dominated by the resonance between downstream and upstream instability waves having the largest absolute growth rate. Koch (1985), in his investigation of wake flows, suggests that there is a location in the near wake at which instability waves are reflected upstream. The resonance then involves wave reflection from this location and, for example, an upstream solid boundary. In a recent analysis of the cylinder wake, Triantafyllou, Triantafyllou & Chryssostomidis (1986) use the concepts of absolute instability to predict the frequency of the vortex street at two extreme values of Reynolds number.

Monkewitz & Nguyen (1986) classify possible regions of absolute and convective instability in typical flows, and assess the validity of the foregoing resonance models within this framework. Moreover, they impose their own resonance condition, which they term the 'initial resonance criterion': the oscillation of the near-wake is controlled by the first self-sustained resonance that the flow encounters. It is important that their interpretation accommodates the possibility of an initially convective instability immediately downstream of separation, when the shear layer is sufficiently thin.

The purpose of the present investigation is to describe certain features of the disturbance growth in the initial region of the separation shear layer, as yet unexplored above $Re = 150$. In this context, one may raise the issue of whether there is a region of exponential disturbance variation downstream of the body at these higher values of Re, and how it relates to the concept of an absolute instability. Moreover, on the basis of the foregoing discussion in association with figure 1, one intuitively expects that the disturbance fluctuation level in the region near separation of the shear layer will vary substantially due to different amplitudes of upstream influence. This variation in initial fluctuation level has not been addressed. All of these features are related to the formation of the large-scale (major) vortices from the cylinder and provide, in themselves, interesting challenges. However, at higher Reynolds numbers, vortex development occurs at two different scales. There is onset of small-scale instability waves at higher frequency f_{BG}; they are often called 'transition waves' (Gerrard 1978). Their coexistence with the large-scale vortices at f_v must be addressed for a full resolution of the shedding process from circular cylinders. In the following we attempt to clarify certain aspects of these issues.

2. Experimental system and instrumentation

Experiments were carried out in a free-surface water channel having a test section 30.5 cm wide by 45.7 cm deep (figure 2). In order to minimize endwall effects, cylinders were mounted within a 24.0 cm wide by 122.0 cm long test-section insert, which clipped off the wall boundary layers of the approach flow. To facilitate flow visualization, both the test section and test-section insert were constructed of Plexiglas. The impingement wedge and its carrier shown in figure 2 were employed

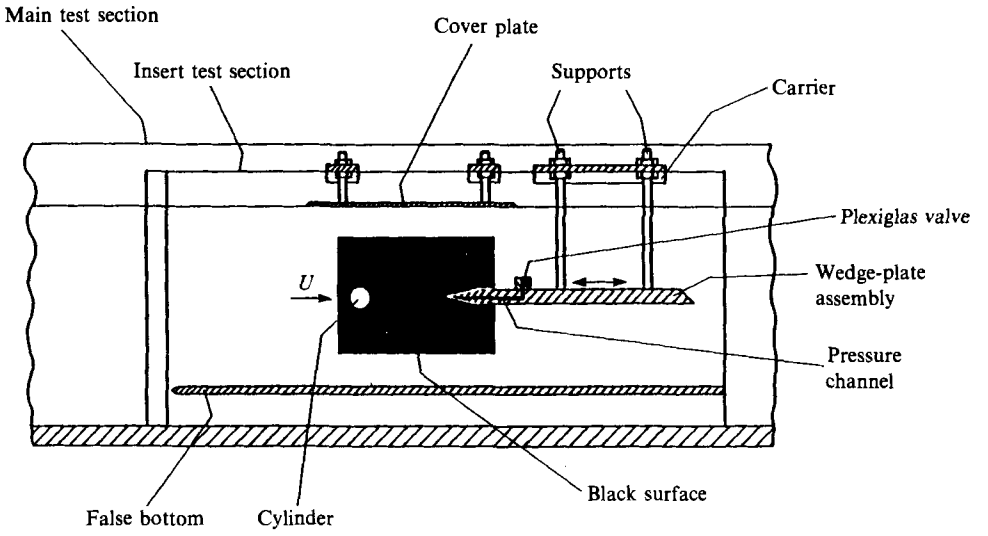

FIGURE 2. Schematic of experimental system.

only in the study described in Part 2; they were removed for the present investigation.

In experiments of this sort involving self-sustained oscillations, parasitic effects of the free surface can arise in the event that one of the free-surface modes of the test section is tuned to the self-generated wake instability of the cylinder. Features of such a coupled resonance have been characterized by Ziada & Rockwell (1983). In order to ensure that such effects were not present in this investigation, a 40.6 cm long cover plate was mounted at the free surface as shown in figure 2. It is also necessary to ensure that the free-stream fluctuation level is minimal, in order to determine the sensitivity of the near-wake region to the upstream influence of the wake-edge interaction. This was accomplished by conditioning the upstream region of the flow in such a manner that the characteristic free-stream velocity fluctuation $\tilde{u}$, relative to the free-stream velocity U, was less than 6×10^{-4}. Moreover, measurements of $\tilde{u}$ in regions away from the cylinder wake instability exhibited an exponential decrease in amplitude as the free stream was approached, thereby indicating absence of free-surface effects.

To cover the range of Reynolds number under consideration, the cylinders had diameters of 0.48, 0.64, 1.28, 1.91 and 2.48 cm. These cylinder diameters corresponded to length to diameter ratios of 50.0, 37.5, 18.8, 12.6 and 9.7. During the course of the experiment, disturbance variations were compared for different values of cylinder length to diameter ratios, to ensure that this parameter did not influence the quantitative growth-rate values. Moreover, in the extreme case of cylinder length to diameter ratio of 9.7, extensive spectra were taken in the spanwise direction to determine the invariance of the time-averaged spectral amplitudes of the large- and small-scale instabilities from the cylinder. In this extreme case, it was found that the central 85% of the flow had essentially the same spectral characteristics, used in constructing the disturbance growth rates. The persistence of consistent patterns of vortex formation for the range of cylinder scale and aspect ratio employed herein is quantified subsequently.

The velocity measurements were carried out using a Disa hot-film probe (55R11)

in conjunction with a Disa anemometer (55D01) and linearizer (55D10). The position of the probe was controlled by a traversing mechanism operated using a stepping motor interfaced with a DEC-MINC or 11-23 minicomputer. The stepping motor provided resolutions in probe displacement in the cross-stream and streamwise directions of 0.91 mm and 1.06 mm respectively. Spectral analysis of the velocity signals was carried out using a fast Fourier transform (FFT). In order to optimize the statistical validity of the spectral amplitudes, up to 15 spectra were averaged at each location. Based on the number of points sampled (from 1024 to 2048), this corresponds to approximately 300 cycles of the large-scale shedding frequency of interest herein.

Pressure measurements were made (in the investigation described in Part 2) with a Kulite XCS-190-2D pressure transducer. The leading edge of the impingement plate allowed measurement of the pressure fluctuations on the upper and the lower surface of the edge at a location near the tip of the edge, $x' = 0.1$ cm, where x' is distance downstream of the tip of the leading edge. These surface pressure taps were connected via channels to a Plexiglas valve in which the pressure transducer was mounted (figure 2). Frequency-response tests show that amplitude and phase distortion due to the finite volume between the sensing surface of the transducer and the pressure tap in the surface of the edge was negligibly small, i.e. 4% and 1.6° at the highest frequency of interest.

As a complement to the foregoing measurements, visualization was carried out using hydrogen-bubble and dye-injection techniques. The hydrogen-bubble technique involved a vertical platinum wire (25 μm in thickness) mounted in a vertical probe holder; a pulsating voltage applied to the wire provided timelines of desired frequency and pulse width. Illumination of the hydrogen-bubble wires involved use of a pair of 90 W stroboscopic lights (Instrobe 90) having a flash duration of 10 μs and operating at a frequency of 120 Hz. In order to optimize the bubble contrast, the vertical wall of the channel directly behind the region of interest was covered by a sheet of flat black construction paper. In the case of dye injection, lighting was from the far side of the test section through a sheet of white, translucent plastic that effectively diffused the light from the two (1000 W) constant-intensity sources.

Visualization was recorded on the Instar television system. This system has vertical and horizontal sweep frequencies of 120 Hz and 25.2 kHz, a resolution of 250 lines, and a framing rate of 120 frames per second. Photos were obtained by photographing the image on the video screen using a 35 mm Nikon F-3 camera.

3. Visualization of flow regimes

Figure 3 shows flow visualization of the vortex development within the range of Reynolds number examined herein. The hydrogen-bubble wire was located near the upstream stagnation point of the cylinder, and pulsed bubbles were generated to provide timeline markers. Figure 3(*a*) shows that as the Reynolds number increases from 270 to 1360, the vortex formation length increases. (This formation length is defined as the distance downstream of the cylinder at which irrotational fluid is drawn across the centreline. It is not necessarily the same as the traditional l_f shown in figure 1.) The trend of increasing formation length in figure 3(*a*) corresponds to a decrease in magnitude of negative base pressure coefficient (see figure 1*c*), summarized by Roshko & Fiszdon (1969). In figure 3(*b*), an increase of the Reynolds number from 1900 to 5040 shows that the formation length decreases; this trend corresponds to an increase in negative base pressure coefficient (also see figure 1*c* and

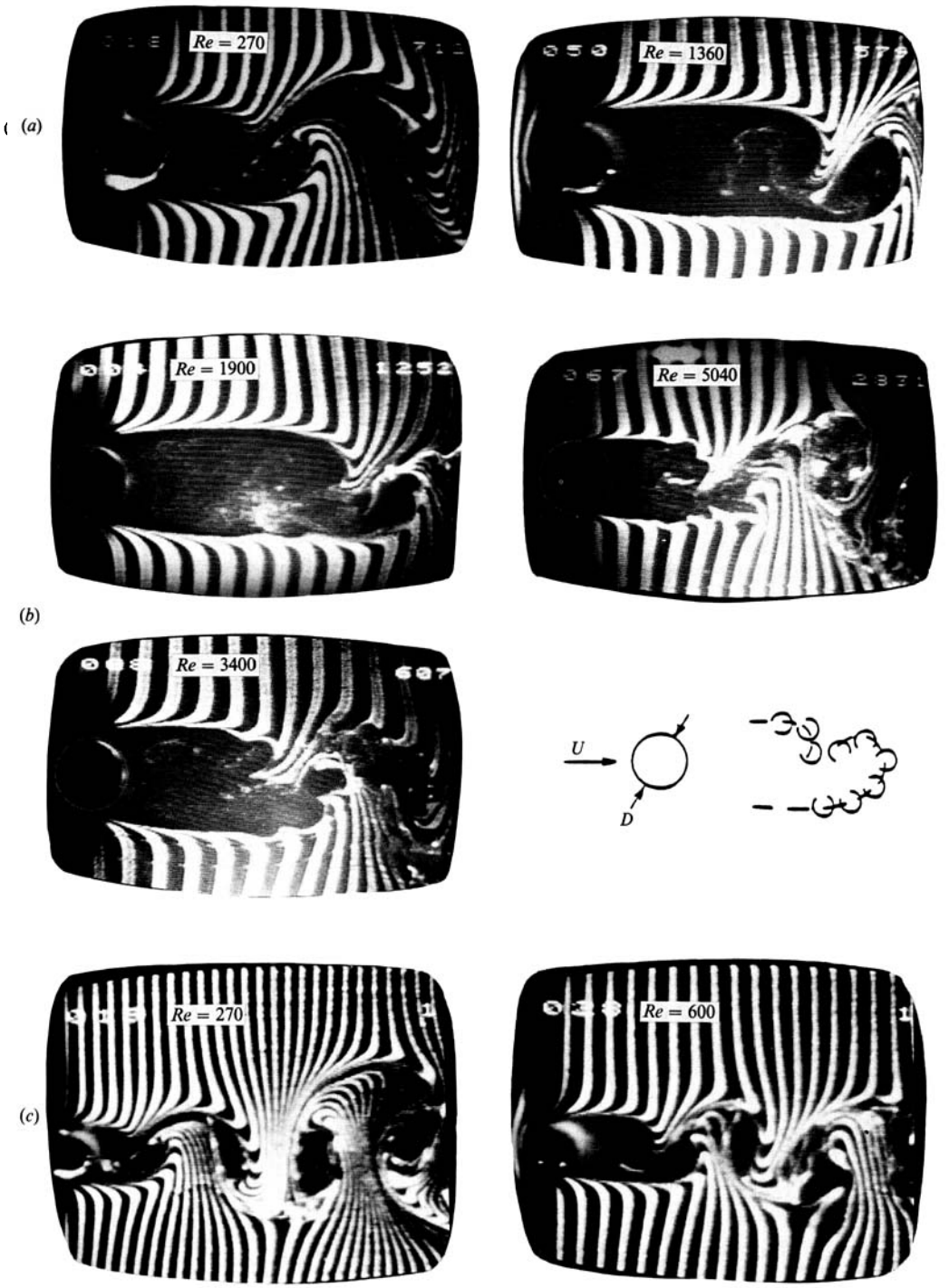

FIGURE 3. (*a*) Variation of near-wake structure in lower Reynolds-number range where absolute value of base pressure coefficient decreases with increasing Reynolds number. (*b*) Near-wake structure over Reynolds-number range where absolute value of base pressure coefficient shows an increase with increasing Reynolds number. (*c*) Wake structure downstream of initial vortex formation showing increase of vortex formation length and narrowing of near wake with increase of Reynolds number.

Roshko & Fiszdon 1969). These observations are linked to an increase in rate of growth of the separating shear layer. At $Re = 3400$ and 5040 the streamwise gradients of shear-layer momentum thickness θ were measured to be $d\theta/dx = 0.028$ and 0.045 respectively. Enhanced entrainment of the shear layer and increased magnitude of negative base pressure are apparently interdependent phenomena.

At Reynolds numbers of about 1900 and above, small-scale instabilities (hereafter referred to as Bloor–Gerrard instabilities) are evident; they become particularly pronounced at $Re = 3400$ and 5040. We note that location of the bubble wire at the downstream side of the cylinder provides little information beyond that shown in figures 3(*a*) and 3(*b*) (A. Ongoren & D. Rockwell, unpublished work, 1986). Onset of Bloor–Gerrard instabilities is not apparent for $Re < 1900$. Moreover, corresponding velocity spectra showed existence of the frequency component corresponding to the small-scale instability only for Re above about 1900.

In figure 3(*c*), covering the lower Reynolds-number range, an increase in Reynolds number appears to narrow the cross-stream extent of the downstream region of the wake and decrease the scale of the downstream vortices, evident from comparison of the right-hand region of photos of $Re = 270$ and 600. This change in the wake structure is associated with onset of pronounced three-dimensionality in the downstream domain of the wake (A. Ongoren & D. Rockwell, unpublished work, 1986). In fact, the increase in vortex formation length evident in figures 3(*a*) and 3(*c*) is compatible with the onset of this three-dimensionality. It may substantially reduce the upstream influence of the quasi-two-dimensional vortex, thereby decreasing the initial fluctuation level near separation. Competition between symmetrical and antisymmetrical modes of the wake instability does not appear to play a role; cross-spectra using hot-film probes on either side of the near wake showed a consistent difference of π.

Unal (1985) discusses possible deviations from the antisymmetrical mode of vortex formation shown in figure 3(*a–c*). At certain values of Re and cylinder aspect ratio, it was possible to induce an intermittent, but relatively infrequent, appearance of a symmetrical mode of vortex formation. For all quantitative studies described herein, however, the antisymmetrical mode was found to persist over a minimum of 92% of the oscillation cycles.

4. Fluctuation level at trailing-end of cylinder as a function of Reynolds number

The initial fluctuation level at or near shear-layer separation is important in identifying whether the initial growth of the disturbance is truly linear or nonlinear, as discussed in §1. In characterizing this initial level, it is most appropriate to select a location very near or at shear-layer separation. Herein, we select a reference fluctuation level at a fixed reference location downstream of shear-layer separation; its location accounts for the fact that the onset of separation is Reynolds-number dependent and that accurate measurements near the surface of the cylinder are difficult. (For values of fluctuation level measured near separation, the reader is referred to subsequent figures.)

To describe this reference fluctuation level, we select transverse (y) locations at the edge of and within the separated shear layer and a streamwise location (x) at the trailing-end of the cylinder, $x/D = 0.5$, where x is measured from the centre of the cylinder. Regarding the transverse location of the reference station, the eigenfunction $\tilde{u}(y)$ of the unstable shear layer shows strong transverse gradients of fluctuation

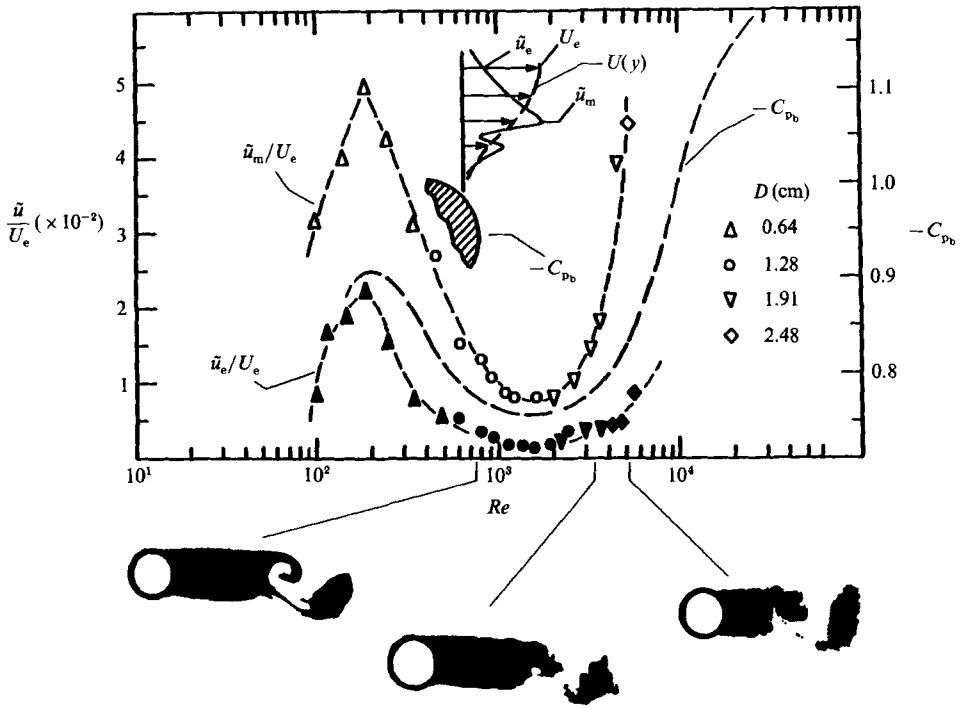

FIGURE 4. Variation with Reynolds number Re of mean base pressure coefficient C_{p_b} and velocity fluctuation amplitudes measured at edge of $(\tilde{u}_e/U_e)$ and at maximum amplitude location within $(\tilde{u}_m/U_e)$ the shear layer at $x/D = 0.5$. Also shown are visualizations of the near-wake structure from dye injection in the base region. Base pressure line is from Roshko & Fiszdon (1969).

amplitude; it is customary to employ either the maximum fluctuation amplitude $\tilde{u}_{max} \equiv \tilde{u}_m$, the value of fluctuation amplitude $\tilde{u}_e$ at the edge of the shear layer where $U = U_e$ (see figure 4), or the integrated kinetic energy across the shear layer $E_{\tilde{u}}$. For the present characterization, we employ the first two parameters, as defined in figure 4. Within the Reynolds-number range considered herein, the momentum thickness θ of the separating shear layer is the order of a few per cent of the cylinder diameter D. (This momentum thickness is evaluated in the traditional fashion (Freymuth 1966).) Consequently, in the schematic of figure 4, the thickness of the shear layer is exaggerated relative to the diameter of the cylinder.

The variations of mean base pressure coefficient C_{p_b} with Reynolds number Re of figure 1 is reproduced in figure 4; it is compared with reference fluctuation levels $\tilde{u}_m/U_e$ and $\tilde{u}_e/U_e$. Both of these fluctuation levels generally follow the trend of the absolute value of base pressure coefficient. Moreover, these levels are inversely related to the visualized vortex formation length, evident in the visualization of figure 3 (*a–c*).

5. Streamwise variation of disturbance amplitude

In determining the amplitude variation of the disturbance in the separating shear layer, one may track the amplitude of the maximum fluctuation $\tilde{u}_m$, the fluctuation amplitude at the edge of the shear layer $\tilde{u}_e$, or the integrated kinetic energy across

the shear layer $E_{\tilde{u}}$. These parameters are illustrated in the inset of figure 5. Moreover, the mean velocity $U(y)$, its value U_e at the edge of the shear layer and the local momentum thickness θ of the shear layer are indicated therein.

Figure 5(*a*) shows the variation of normalized fluctuation amplitude $\tilde{u}_e/(\tilde{u}_e)_0$ at the edge of the shear layer as a function of absolute distance x for extreme values of Reynolds number Re and diameter D; $(\tilde{u}_e)_0$ is the value extrapolated to $x = 0$. In terms of the absolute streamwise distance x, the disturbance amplitude varies substantially with D; however, in all cases, there is a well-defined exponential variation.

Figure 5(*b*) demonstrates the equivalence between fluctuation level at the edge of the shear layer $\tilde{u}_e/U_e$ and the square root of the integrated kinetic energy

$$E^*_{\tilde{u}} \equiv \left(\frac{1}{2}\int \frac{\tilde{u}^2(y)}{U_e^2 \theta_m}\,dy\right)^{\frac{1}{2}},$$

in interpreting the amplitude variation. In doing so, we employ the characteristic momentum thickness θ_m at the middle of the exponential growth region. It is evident from figure 5(*b*) that over the sevenfold range of Reynolds number considered herein, the streamwise amplitude variation is essentially the same, at a given Re, whether one employs the concept of integrated kinetic energy $E^*_{\tilde{u}}$ or a fluctuation at the edge of the shear layer $\tilde{u}_e$.

In figure 5(*c*), the disturbance amplitude variation is shown for a total of six Reynolds numbers and varying initial fluctuation level. Over this Reynolds-number range, the slopes of the curves deviate by about 15% from the mean value, while the initial fluctuation level changes by about a factor of three. In figure 5(*d*), the velocity amplitude $\tilde{u}_e$ and integrated kinetic energy $E^*_{\tilde{u}}$ are normalized with respect to their initial values. The primary cause of the deviations in amplitude variation is most likely to be due to the fact that these variations are correlated with a single lengthscale θ_m, which is strictly appropriate only for a parallel flow.

6. Small-scale disturbances in unstable shear layer

Extensive spectra of $\tilde{u}$ taken within the shear layer over a range of streamwise locations show that, in general, there are two predominant spectral components: that corresponding to the primary vortex shedding frequency f_v described in the foregoing; and that of a smaller-scale instability, often referred to in the literature as a 'transition wave', which we designate as the Bloor–Gerrard frequency f_{BG} (Bloor 1964; Gerrard 1978). At arbitrary locations in the shear layer, Bloor (1964) and Wei & Smith (1986) have found $f_{BG}/f_v \propto (Re)^k$, where $k = 0.5$ and 0.87 respectively. As shown by Unal (1985), the characteristic thickness of the unstable shear layer does not follow that expected from laminar considerations, i.e. $\theta_m \propto 1/Re^{\frac{1}{2}}$, so we do not expect

---

FIGURE 5. (*a*) Variation of velocity fluctuation at edge of shear layer $\tilde{u}_e/(\tilde{u}_e)_0$ for various cylinders of diameter D; and (*b*) variation of velocity fluctuation amplitude at edge of shear layer $\tilde{u}_e/U_e$ and integrated kinetic energy parameter $E^*_{\tilde{u}}$ as a function of downstream distance x/θ_m, with momentum thickness θ at middle of exponential growth region used as a normalizing length. (*c*) Amplitude variation of fluctuation amplitude at edge of shear layer $\tilde{u}_e/U_e$ as a function of Reynolds number Re; (*d*) variation of normalized amplitude of fluctuation at edge of shear layer $\tilde{u}_e/(\tilde{u}_e)_0$ and integrated kinetic energy parameter $E^*_{\tilde{u}}/(E^*_{\tilde{u}})_0$ for a range of Reynolds number as a function of streamwise distance x/θ_m where θ_m is momentum thickness at middle of each respective exponential growth region.

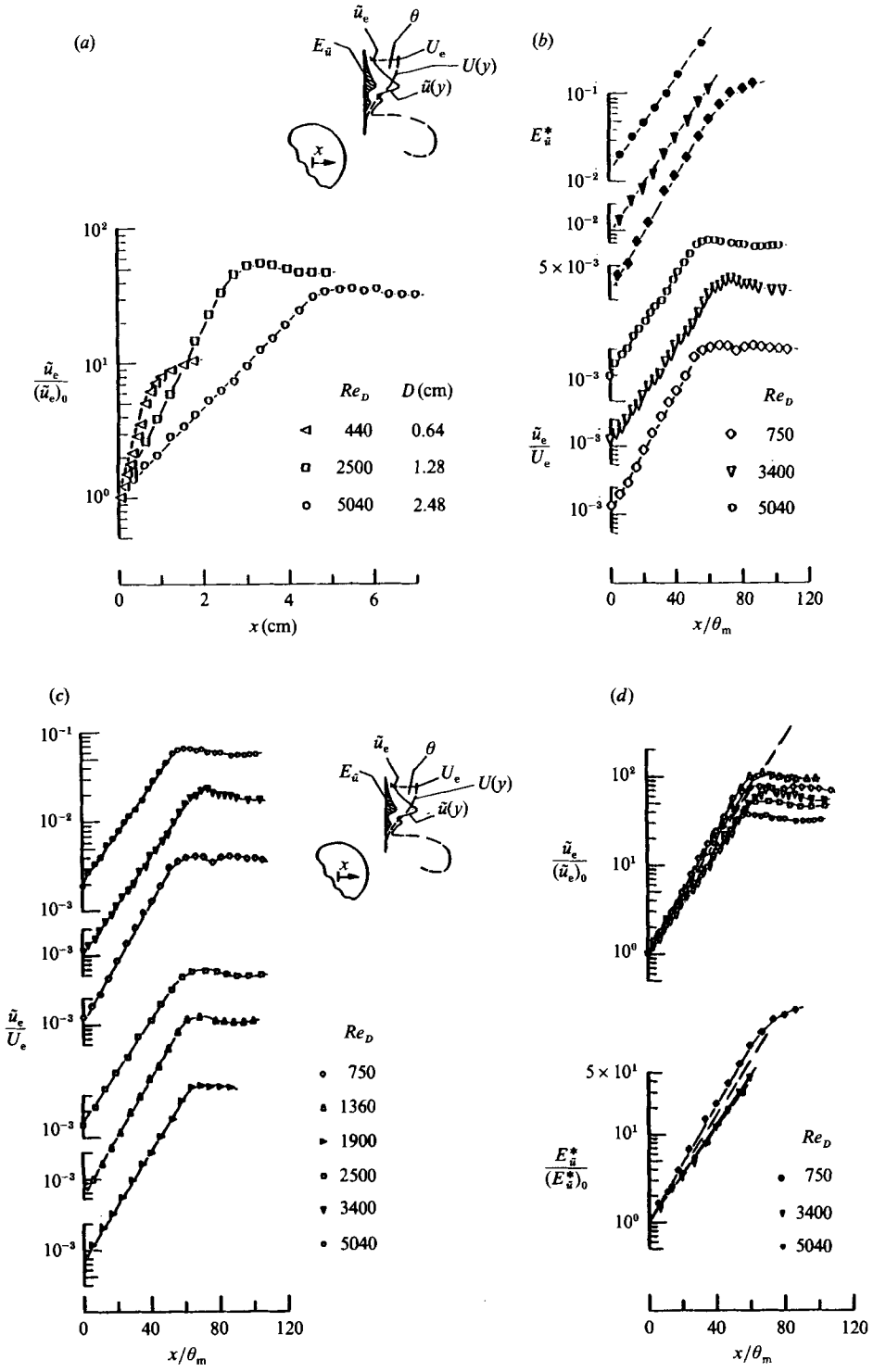

FIGURE 5 (*a–d*). For caption see facing page.

f_{BG} to scale according to a laminar shear-layer thickness over the range of Re considered herein.

In this investigation, below $Re = 1900$, only the component f_v was detectable; above this value, both f_v and f_{BG} were present, with contributions from f_v extending over the entire streamwise extent of the shear layer, and contributions from f_{BG} being detectable over a limited streamwise extent. In general, this high-frequency component f_{BG} is more difficult to quantify, a feature most likely to be connected to rapid onset of small-scale spanwise instabilities of the shear layer (Gerrard 1978; Wei & Smith 1986).

Figure 6 shows a typical family of frequency spectra of $\tilde{u}$, with predominant spectral components at f_v and f_{BG}, taken across the shear layer at a streamwise station shortly downstream of shear-layer separation. At this station, the energy level E_u^* of the high-frequency instability (at f_{BG}) is maximum. These spectra emphasize that the relative amplitudes of the components at f_v and f_{BG} are a strong function of transverse (y) location within the shear layer, the component at f_v dominating in the lower part and that at f_{BG} in the upper part. Also evident in figure 6 are other frequency components corresponding to higher harmonics of f_v, i.e. $2f_v$ and $3f_v$, as well as components arising from nonlinear interaction between f_v and f_{BG}, i.e. $f_{BG}+f_v$ and $f_{BG}-f_v$. It is important that in these spectra, as well as in those acquired further upstream and downstream, there occurs no pronounced subharmonic(s) of the small-scale instability f_{BG}. This observation is in contrast to what is expected from free mixing-layer studies (Roshko 1976), where successive vortex pairing of small-scale instabilities gives rise to large-scale instabilities. In this respect, the developing shear layer of the cylinder near wake is distinctly different from a free mixing layer. Visualization suggests that the f_{BG} vortices simply form a frill upon the large-scale f_v vortex. However, in the event that the large-scale vortex formation in the cylinder wake is artificially suppressed by insertion of a splitter plate (Unal 1985), successive vortex pairing and corresponding generation of subharmonic components does occur.

Figure 7 shows amplitude variations corresponding to the maximum fluctuation level $\tilde{u}_m/U_e$ within the shear layer and the dimensionless square root of the kinetic energy $E_{\tilde{u}}^*$, both at the frequency of large-scale vortex shedding f_v. In addition, the kinetic energies $E_{\tilde{u}}^*$ for the component f_{BG} are also given. At $Re = 750$, there is no detectable small-scale instability at f_{BG}. In this case, the amplitude of the maximum fluctuation within the shear layer follows that of the square root of the integrated energy. At higher values of $Re = 3400$ and 5040, there is distortion of the variation of the maximum amplitude of the fluctuation component $\tilde{u}_m$ relative to the exponential variation of energy $E_{\tilde{u}}^*$ at frequency f_v (Unal & Rockwell 1984). This distortion occurs over streamwise distances for which there are detectably large amplitudes of the high-frequency instability component f_{BG}. Comparing with the visualization of figure 3 (b) at $Re = 3400$ and 5040, there is clearly an interrelationship between the large-scale vortex-formation length therein and initial fluctuation levels $[\tilde{u}_m/U_e]_{x/\theta_m=0}$ and $[E_{\tilde{u}}^*]_{x/\theta_m=0}$: formation length decreases and initial fluctuation level increases. In fact, artificial suppression of the development of the downstream vortex street via a splitter plate drastically decreases the initial fluctuation level (Unal & Rockwell 1987).

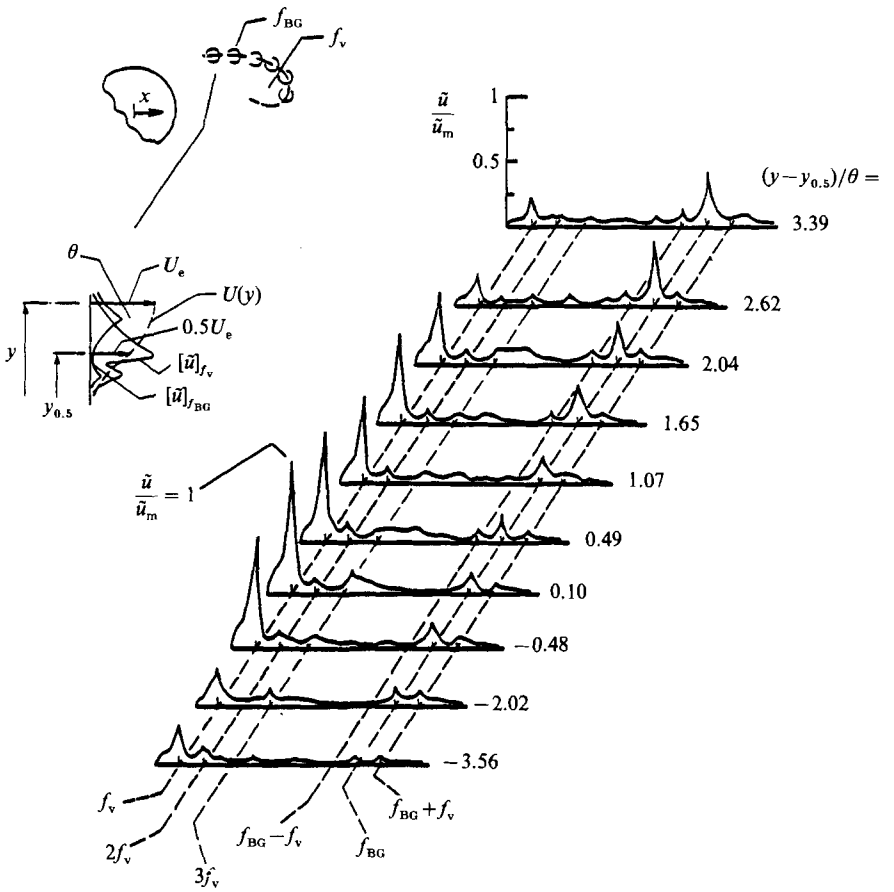

FIGURE 6. Spectra of velocity fluctuation amplitude taken across shear layer at $x/D = 1.25$ and $Re = 5040$. The primary, large-scale vortex shedding frequency is f_v and the small-scale instability frequency is f_{BG}.

7. Disturbance amplification rates

From the regions of exponential disturbance growth of figure 5, one may determine the amplification rate $-k_i$ in accord with

$$-k_i = -k_i' y_{0.5} = \ln(\tilde{u}/\tilde{u}_0)/(x/y_{0.5}),$$

in which $y_{0.5}(x)$ is the distance from the wake centreline to the half velocity ($U = 0.5U_e$) of the wake and $\tilde{u}_0$ is the characteristic velocity fluctuation amplitude at $x = 0$. Data for three values of Reynolds number $Re = 750$, 3400, 5040 are shown in figure 8(*b–d*) as solid symbols.

We compare these data with spatial stability calculations of P. Monkewitz (private communication, 1986). In the plane of amplification factor $-k_i$ versus vorticity-thickness δ_ω parameter N^{-1}, where $N^{-1} \approx \delta_\omega \sinh^{-1} 1/(\sqrt{2}y_{0.5})$, there are, due to the absolute nature of the instability, two families of theoretical curves (figure 8*a*) in accord with the existence of downstream and upstream modes. Each curve has been computed for a constant value of real frequency $\omega = 2\pi f y_{0.5}/(\frac{1}{2}U_e)$.

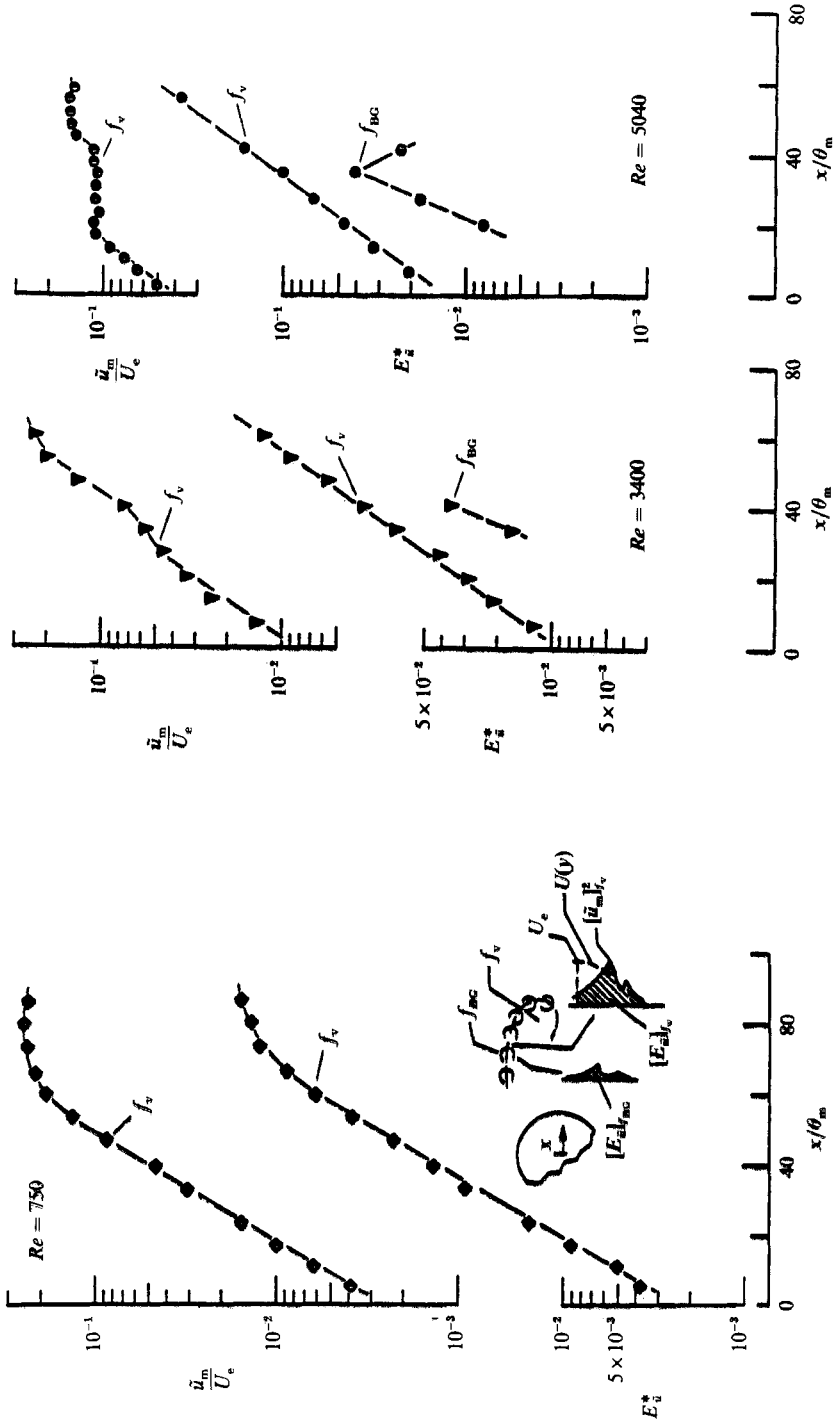

FIGURE 7. Variation of maximum amplitude of velocity fluctuation within shear layer $\tilde{u}_m/\bar{U}_e$ and integrated kinetic energy parameter $E_{\tilde{u}}^*$ at large-scale shedding frequency f_v and small-scale instability frequency f_{BG} over a range of Reynolds number $Re \equiv UD/\nu$.

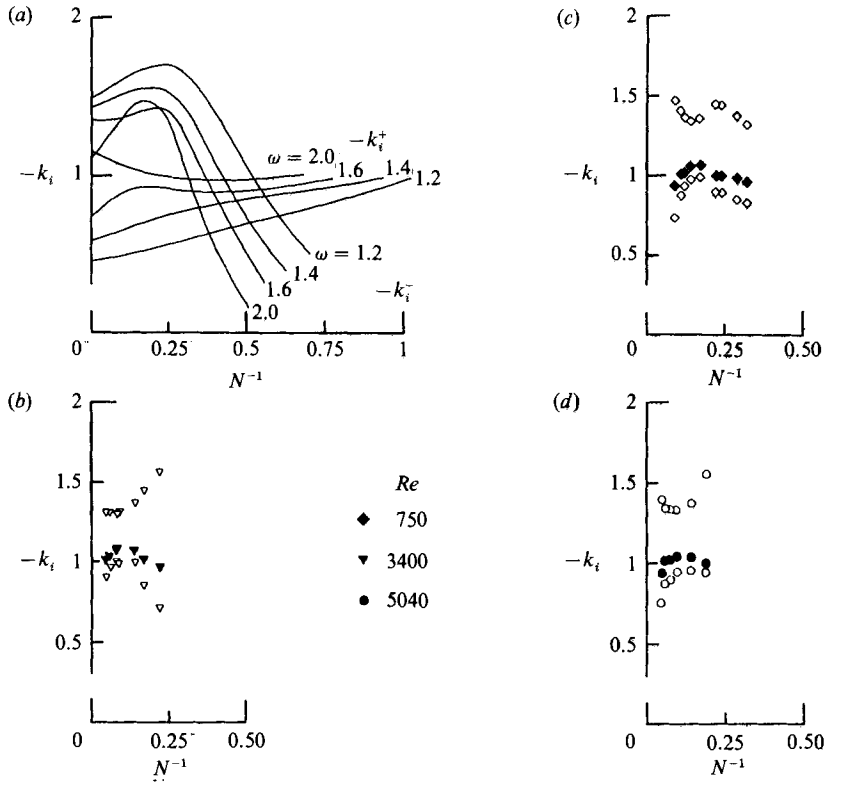

FIGURE 8. Comparison of experimental (closed symbols) and theoretical (open symbols) growth rates $-k_i$ *vs.* dimensionless vorticity thickness of shear layer N^{-1} with frequency ω as parameter. Theoretical curves calculated by P. Monkewitz (private communication, 1986).

The experimental data, given by the solid symbols in figure 8(*b–d*), correspond to a wide range of dimensionless vorticity thickness $0.046 < N^{-1} < 0.30$; these data fall within the frequency range $1.5 < \omega < 1.8$. At each experimental value of N^{-1} and ω, we determine, from figure 8(*a*), the theoretical values of amplification factor $-k_i$ corresponding to the two instability modes. These theoretical values are indicated by the open symbols in figure 8(*b–d*). At all values of Reynolds number, the trend of $-k_i$ *vs.* N^{-1} is best approximated by the lower set of theoretical points, believed to correspond to the downstream mode. We emphasize, however, that the distinction between upstream and downstream modes is not clearcut in an absolutely unstable flow.

Figure 9 further compares the data of figure 8 on the $-k_i$ *vs.* ω plane with N as a parameter. Calculations are for $N = 2, 5, 10$; note that the data correspond to $N > 3.3$ (see figure 8). As expected from figure 8, the calculations approximate well to the data trend.

Most important, however, is the correspondence between the range of ω covered by the data and that by vertical arrows. These arrows represent the frequencies (for the values of $N = 2, 5, 10$) at which local self-sustained resonances are possible in the wake. The spread of the data over a finite range of ω is due, of course, to the variations of $y_{0.5}(x)$ over the streamwise extent of the exponential growth region. Since the stability analysis is based on parallel flow concepts, choice of the most

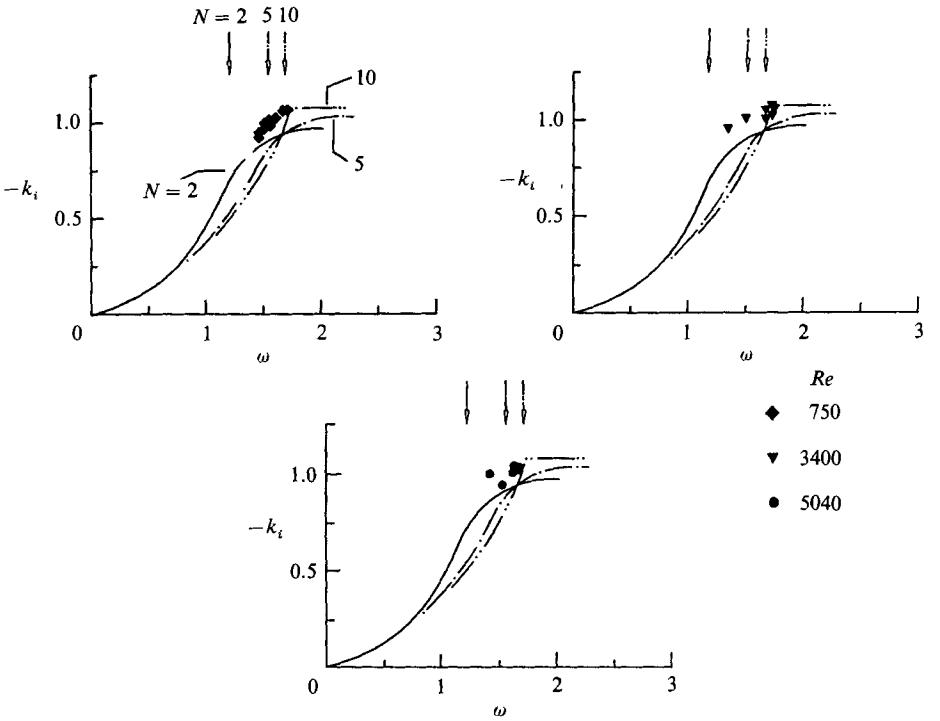

FIGURE 9. Comparison of $-k_i$ *vs.* ω for three values of $N = 2, 5, 10$. Arrows denote branch point frequencies at these values of ω from calculations of Monkewitz & Nguyen (1986).

representative $y_{0.5}$ is somewhat subjective, and must be made with care. For this reason, we show in figure 9 the entire span of data of figure 8, rather than attempting to match most favourably with theory.

Considering the overall plot of figure 9, we note that the curve corresponding to $N = 10$ is very similar to that of $N = \infty$. It represents, in essence, the lower portion of the spatial stability curve for a single shear layer (Michalke 1965), and its maximum amplification rate occurs at $\omega \approx 5.1$ (Monkewitz & Nguyen 1986). At successively lower values of N, i.e. $N = 5$ and 2, the value of ω at which maximum amplification occurs moves to substantially lower values. Thus, on the basis of maximum disturbance amplification, one would expect the wake oscillation frequency to vary substantially with the thickness of the separating shear layer, i.e. with N^{-1}. However, the clustering of the data close to the branch point frequencies (arrows of figure 9) clearly suggests that the controlling mechanism of the wake oscillation is a resonance of the type postulated by Betchov & Criminale (1966), Koch (1985), and Monkewitz & Nguyen (1986).

Comparison of theoretical and experimental mean velocity profiles and eigenfunctions is given in figure 10. Data correspond to the middle of the exponential growth region at each value of Reynolds number. This corresponds, over the range of Re, to $1.0 < x/D < 1.4$, $1.65 < \omega < 1.69$, $5.8 < N < 7.0$. The mean velocity distributions are compared to the functional form

$$U/U_e = 1 - [1 + \sinh^{2N}(y/y_{0.5} \sinh^{-1} 0.9734)]^{-1},$$

for $N = 6.4$. Regarding the eigenfunction $\tilde{u}/\tilde{u}_m$ comparison, all data are compared

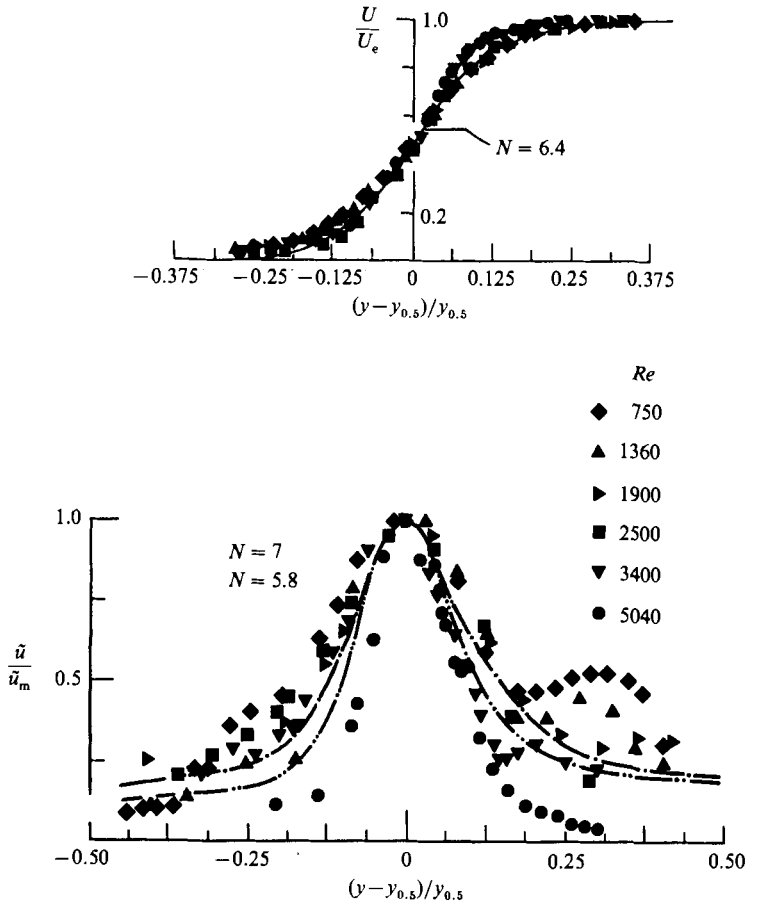

FIGURE 10. (*a*) Comparison of mean velocity distribution across shear layer with the theoretical distribution (Monkewitz & Nguyen 1986); (*b*) comparison of eigenfunction distribution calculated by P. Monkewitz (private communication, 1986) with data.

with theoretical distributions of the downstream mode of $N = 5.8$ and 7.0. Although the general form of the data follows that of the theory, there are large deviations at the extreme values of $Re = 750$ and 5040.

The agreement of the data with the theoretical eigenfunction of the upstream mode (not shown here) is less favourable. There occurs a minimum of $\tilde{u}/\tilde{u}_m$ at about $(y-y_{0.5})/y_{0.5} - 0.19$, followed by a rise to another (smaller) maximum amplitude at larger negative y, i.e. at $(y-y_{0.5})/y_{0.5} \approx -0.35$.

8. Concluding remarks

For the range of Reynolds number considered herein, the flow structure behind the cylinder undergoes a drastic alteration as it passes from a quasi-laminar instability to one in which there are two distinctly different scales of instability. The variations in base pressure, vortex strength, and formation length with Reynolds number are substantial, as revealed in a number of previous investigations. In this investigation, we have attempted to interpret these traditional parameters within the context of unstable shear layers from the cylinder.

In the event that the separating shear layer supports a purely convective instability, one may view the initial fluctuation level (near separation) to be a direct function of the upstream-induced velocity/pressure fields. In general, via Biot-Savart induction, the largest initial fluctuation levels would be associated with the smallest values of vortex-formation length. The importance of accounting for upstream influence is also emphasized by Michalke (1984) in his assessment of jet instabilities. As discussed therein, the self-excited frequency of a jet instability is substantially lower than that predicted by spatial theory. Aside from the possible influence of non-parallel effects, Michalke suggests that the downstream vorticity dynamics may control the preferred frequency. Considering the area integral of the fluctuating vorticity (centred at a distance x_0 from the separation edge) to evaluate the circulation Γ over a disturbance wavelength λ, the magnitude of the upstream induced velocity is proportional to $|\Gamma|/\lambda U_0$ and, where U_0 is the stream velocity at the edge of the layer, has a maximum at a frequency close to that of the most amplified disturbance from experiments, but substantially lower than that of the most amplified from spatial theory. Accordingly, we would expect compatibility between the most amplified disturbance in the shear layer from the cylinder and the downstream vorticity dynamics.

However, there is another type of upstream influence that may potentially exert a strong, if not the controlling, influence: upstream wave motion due to the existence of an absolute instability in the near wake (Koch 1985; Monkewitz & Nguyen 1986). Interpretation of experimental data on disturbance growth rates and eigenfunctions within the framework of absolute instability is complicated on several fronts. First of all, both upstream and downstream modes exist. It is necessary to know the relative amplitudes of these modes in comparing experiment with theory; in certain situations, however, it may be possible to demonstrate that one of these modes dominates. Second, the relative amplitude of modes will be a function of streamwise distance along the shear layer. This feature, along with the usual assumptions in applying parallel stability theory to non-parallel flows (Ho & Huerre 1984), complicates the interpretation. Finally, there is the issue of whether it is most appropriate to analyse the absolute instability using: real frequency ω as done herein; or complex frequency $\omega = \omega_r + i\omega_i$, accommodating a global growth rate ω_i (P. Monkewitz private communication, 1986).

We emphasize that the fluctuation levels of the instability near separation are, over certain ranges of Reynolds number, very large. Indeed, this fluctuation level takes on values much higher than those typically achieved in purely hydrodynamic oscillations of jets and mixing layers where no acoustic resonance or fluid-elastic effects come into play (Rockwell 1983). The issue remains as to the relative predominance of upstream influence through: Biot-Savart induction; and upstream influence from the region of absolute instability.

Moreover, we emphasize another class of approximations that has been employed in comparing experiment with theory. In a rigorous sense, one must account for the nonlinear character of the disturbance. Nonlinearity is evident in the relatively high fluctuation levels at separation (figures 4 and 7). Furthermore, the non-parallelism of the mean shear layer, evidenced by $\theta(x)$, arises from the Reynolds stresses, which in turn are a higher-order product of the velocity perturbation, requiring accommodation of nonlinearity. An additional complication arises from the simultaneous existence of large-scale (f_v) and smaller-scale (f_{BG}) components. In the spirit of unstable wave growth in fully turbulent flows (Wygnanski & Petersen 1985), we may view the growth of the wave at f_v in presence of the f_{BG} instability (which

may be three-dimensional) as a degenerate case of organized wave growth in a turbulent flow. In fact, as noted by Wygnanski & Petersen (1985), the small-scale motions do not exert a substantial influence on the macroscale dynamics of the flow. In essence, we view the growth of the smaller-scale instabilities at f_{BG}, as well as that at f_v, as contributing to the thickening of the mean shear layer, i.e. $\theta(x)$. This thickened shear layer, however, then serves as the base mean flow for a quasi-linear description of the disturbance development at f_v, again following the principles of organized wave growth in turbulent flow.

In the foregoing we have addressed the nature of the instability leading to the classical, Kármán vortex street. As noted herein, as well as in a number of previous studies, small-scale Bloor–Gerrard vortices can exist in the separating shear layer at sufficiently high Reynolds number. Particularly remarkable is the fact that there is no evidence of successive coalescence of the Bloor–Gerrard vortices at f_{BG}. In the corresponding free jet or mixing layer, one observes successive pairing of neighbouring vortices to produce large-scale structures in downstream regions of the flow (Roshko 1976). A relevant case for comparison involves the transition of an axisymmetric jet, which involves two distinct instability modes, one associated with the small-scale thin shear-layer instability and the other associated with a large-scale stability of the jet (Kibens 1980). As demonstrated by Kibens, successive pairing of small-scale vortices leads to large-scale vortices compatible with a column-type instability mode. In contrast, extensive spectra taken throughout the two-scale mixing layer herein shows no evidence of successive subharmonics of the Bloor–Gerrard frequency; this quantitative result, along with flow visualization suggests that the small-scale vortices form a frill upon large-scale vortices. In fact, one may make the interesting observation that as Reynolds number increases the initial fluctuation level near the upstream separation increases as well.

It is well known, from previous experiments on jets (Rockwell 1972) and mixing layers (Ho 1981) subjected to relatively high amplitude initial disturbance levels, that successive vortex pairing does not occur, but instead there is 'forced fusion' (Rockwell 1972) or 'collective coalescence' (Ho 1981). This phenomenon appears to be most analogous to that occurring in the two-scale mixing layer herein. That is, as the number of Bloor–Gerrard vortices increases, the initial excitation level increases as well. This ensures that the small-scale vortices coalesce together during formation of the large-scale vortex.

Another feature of the unstable shear layer that distinguishes it from its classical counterpart is dominance of the fluctuating kinetic-energy at the large-scale vortex-formation frequency f_v over that at the small-scale frequency f_{BG}. This dominance persists from separation onwards. In accord with the aforementioned lack of detection of subharmonics of f_{BG}, there is not successive energy transfer from smaller to larger scales as the shear layer evolves in the streamwise direction. We suggest that this dominance of energy at f_v is due to pronounced upstream influence from Biot-Savart induction, existence of an absolute instability, or a combination of them.

'Transition waves' were not observed for $Re < 1900$, in contrast to Gerrard (1978), who observed them to extend well below this value. Among the factors that could influence the initial fluctuation level and growth of these waves are the background noise of the facility in the spectral range of the instability wave, the cylinder aspect ratio, and the nature of cylinder end conditions. Concerning aspect ratio effects, we note that Gerrard's (1978) observations of the well-defined symmetric mode at $Re = 1968$ were apparently at a cylinder aspect ratio $L_c/D = 14$. As shown by Unal (1985),

decreasing the cylinder aspect ratio at $Re = 1360$ (corresponding to the minimum in the base pressure curve) to $L_c/D = 12.6$ does in fact substantially increase the fraction of time that the symmetric mode is present.

There is insufficient evidence to generalize the occurrence or non-occurrence of the symmetric mode as a function of cylinder aspect ratio. Clearly, this aspect is worthy of further study. In this regard, it should be pointed out that the effects of cylinder end conditions on the wake dynamics are not well understood. Although one might view a larger cylinder aspect ratio as promoting greater three-dimensionality, the study of Graham (1969) at Re of the order of 10^4 shows that the end plates on a D-shaped cylinder produce two-dimensional shedding only if the distance between the plates is less than or equal to four cylinder widths, a distance most likely associated with the spanwise scale of the 'cells' that would exist on an infinitely long cylinder. Zdravkovich (1986) provides a review of extensive data on spanwise correlation length in the downstream wake over a range of Reynolds number. Of course, in general, one expects these correlations to be a function of streamwise distance and transverse location in the shear-layer. Gerich & Eckelmann (1982) assess a range of studies confronting the subtleties of end effects and carry out experiments at very low Re demonstrating existence of two shedding frequencies, one in the core region and another near the endwall/plate wall, the former being about 10–15% less than the latter. From the foregoing, as well as our own experience, we believe the cylinder aspect ratio is not simply a geometrical effect. The length scales L_c and D should be considered in relation to the wavelength of the large-scale shedding of λ_v and that of the Bloor–Gerrard instability λ_{BG}.

In the present investigation, it is the antisymmetrical mode of the large-scale vortex formation that dominates; therefore, all of the quantitative data is an accurate reflection of the wake dynamics in this limiting case. In the event that it is possible to induce a persistent symmetrical mode, at the expense of attenuation of the antisymmetrical mode, it may well be possible for coalescence of the adjacent small-scale Bloor-Gerrard vortices to occur. In this case, it is possible that the fluctuating energy of the large-scale vortex shedding would not dominate from separation onwards as demonstrated herein. In fact, as discussed by Unal (1985) and Unal & Rockwell (1987), suppression of the antisymmetrical mode of the large-scale vortex formation by a splitter plate shows a decrease in initial fluctuation level at f_v and well-defined vortex coalescence of the vortices at f_{BG}; shear-layer spectra exhibit a clear subharmonic of f_{BG} in contrast to the free, non-attenuated wake where the antisymmetrical mode of the large-scale vortices at f_v dominates.

The authors gratefully acknowledge primary financial support of the Office of Naval Research. Preliminary flow visualization related to this investigation was aided by funding from the Volkswagen Foundation. The authors are particularly appreciative of discussions with Professor P. Monkewitz, as well as his providing us with unpublished calculations. Engaging discussions with Professor M. V. Morkovin and helpful remarks by Drs J. Gerrard and M. Zdravkovich were of great value in formulating the final draft of this manuscript.

REFERENCES

ABERNATHY, F. H. & KRONAUER, R. E. 1962 The formation of vortex streets. *J. Fluid Mech.* **13**, 1–20.

BEARMAN, P. W. 1967 On vortex street wakes. *J. Fluid Mech.* **28**, 625–641.

BERGER, E. W. & WILLE, R. 1972 Periodic flow phenomena. *Ann. Rev. Fluid Mech.* **4**, 313–340.

BETCHOV, R. & CRIMINALE, W. O. 1966 Spatial instability of the inviscid jet and wake. *Phys. Fluids* **9**, 359–362.

BLEVINS, R. D. 1977 *Flow -Induced Vibration.* Van Nostrand Reinhold.

BLOOR, M. S. 1964 The transition to turbulence in the wake of a circular cylinder. *J. Fluid Mech.* **19**, 290–304.

BLOOR, M. G. & GERRARD, J. H. 1966 Measurements on turbulent vortices in a cylinder wake. *Proc. R. Soc. Lond.* A**294**, 319–342.

FREYMUTH, P. 1966 On transition in a separated boundary layer. *J. Fluid Mech.* **25**, 683–704.

GERICH, D. & ECKELMANN, H. 1982 Influence of end plates and free ends on the shedding frequency of circular cylinders. *J. Fluid Mech.* **122**, 109–121.

GERRARD, J. H. 1966 The mechanics of the formation region of vortices behind bluff bodies. *J. Fluid Mech.* **25**, 401–413.

GERRARD, J. H. 1978 The wakes of cylindrical bluff body at low Reynolds number. *Phil. Trans. R. Soc. Lond.* A**288**, 1354, 351–382.

GRAHAM, J. M. R. 1969 The effect of end-plates on the two-dimensionality of a vortex wake. *Aero. Q.* **20**, 237–247.

GRIFFIN, O. M. & RAMBERG, S. E. 1974 The vortex-street wakes of vibrating cylinders. *J. Fluid Mech.* **66**, 553–576.

HO, C. M. 1981 Local and global dynamics of free shear layer. *Numerical and Physical Aspects of Aerodynamic Flows*, pp. 521–522. Springer.

HO, C. M. & HUERRE, P. 1984 Perturbed free shear layers. *Ann. Rev. Fluid Mech.* **16**, 365–424.

HUERRE, P. & MONKEWITZ, P. A. 1985 Absolute and convective instabilities in free shear layers. *J. Fluid Mech.* **159**, 151–168.

KÁRMÁN, T. VON 1911 Ueber den Mechanismus des Widerstandes, den ein bewegter Koerper in einer Fluessigkeit erfaehrt. *Goettinger Nachrichten, math.-phys. Kl.* 547.

KIBENS, V. 1980 Discrete noise spectrum generated by an acoustically excited jet. *AIAA J.* **18**, 434–441.

KOCH, W. 1985 Local instability characteristics and frequency determination of self-excited wake flows. *J. Sound Vib.* **99**, 53–83.

MICHALKE, A. 1965 On spatially growing disturbances in an inviscid shear layer. *J. Fluid Mech.* **23**, 521–544.

MICHALKE, A. 1984 Survey on jet instability theory. *Prog. Aero. Sci.* **21**, 159–199.

MONKEWITZ, P. & NGUYEN, L. N. 1986 Absolute instability in the near-wake of two-dimensional bluff bodies. *J. Fluids Struct.* **1**, 165–184.

MORKOVIN, M. 1964 Flow around circular cylinders – a kaleidoscope of challenging fluid phenomenon. *ASME Symposium on Fully Separated Flows*, pp. 102–118.

NAKAYA, C. 1976 Instability of near wake behind a circular cylinder. *J. Phys. Soc. Japan* **1**, 1087–1088.

NISHIOKA, M. & SATO, H. 1978 Mechanism of determination of the shedding frequency of vortices behind a cylinder at low Reynolds numbers. *J. Fluid Mech.* **89**, 49–60.

PIERREHUMBERT, R. T. 1984 Local and global baroclinic instability of zonally varying flow. *J. Atmos. Sci.* **41**, 2141–2162.

ROCKWELL, D. 1972 External excitation of planar jets. *Trans. ASME* E: *J. Appl. Mech.* **39**, 883–890.

ROCKWELL, D. 1983 Invited lecture: Oscillations of impinging shear layers. *AIAA J.* **21**, 645–664.

ROSHKO, A. 1954 On the drag and shedding frequency of two-dimensional bluff bodies. *NACA Tech. Note* 3169.

ROSHKO, A. 1976 Structure of turbulent shear flows: A new look. *AIAA J.* **14**, 1349–1357.

ROSHKO, A. & FISZDON, W. 1969 On the persistence of transition in the near-wake. *SIAM J.*, pp. 607–616.

SAFFMAN, P. G. & SCHATZMAN, J. C. 1982 An inviscid model for the vortex street wake. *J. Fluid Mech.* **122**, 467–486.

SARPKAYA, T. 1979 Vortex-induced oscillations. *J. Appl. Mech.* **46**, 241–258.

STROUHAL, V. 1878 Ueber eine besondere Art der Tonerregung. *Annln Phys.* New Ser. **5**, 216–251.

TRIANTAFYLLOU, G. S., TRIANTAFYLLOU, M. S. & CHRYSSOSTOMIDIS, C. 1986 On the formation of vortex streets behind stationary cylinders. *J. Fluid Mech.* **170**, 461–477.

UNAL, M. F. 1985 Vortex formation from bluff and thin trailing-edges. PhD dissertation, Department of Mechanical Engineering and Mechanics, Lehigh University, Bethlehem, Pennsylvania 18015.

UNAL, M. F. & ROCKWELL, D. 1984 On the role of shear layer stability in vortex shedding from cylinders. *Phys. Fluids* **27**, 2598–2599.

UNAL, M. F. & ROCKWELL, D. 1987 On vortex formation from a cylinder. Part 2. Control by splitter-plate interference. *J. Fluid Mech.* **190**, 513–529.

WEI, T. & SMITH, C. R. 1986 Secondary vortices in the wake of circular cylinders. *J. Fluid Mech.* **169**, 513–533.

WILLE, R. 1974 Generation of oscillatory flows, in *Flow Induced Structural Vibrations* (ed. E. Naudascher), pp. 1–16. Springer.

WYGNANSKI, I. & PETERSEN, R. A. 1985 Coherent motion in excited free shear flows. *AIAA Paper* 85-0539 presented at AIAA Shear Flow Control Conference, March 12–14, Boulder, Colorado.

ZIADA, S. & ROCKWELL, D. 1982 Generation of higher harmonics in a self-oscillating mixing layer edge system. *AIAA J.* **20**, 196–202.

ZIADA, S. & ROCKWELL, D. 1983 Subharmonic oscillations of a mixing layer-wedge system associated with free-surface effects. *J. Sound Vib.* **87**, 483–491.

ZDRAVKOVICH, M. 1987 *Flow Past Cylinders.* Springer (in press).